Inhibitory coherence in a heterogeneous population of subthreshold and suprathreshold type-I neurons

2012 J. Phys. A: Math. Theor. 45 155102

(http://iopscience.iop.org/1751-8121/45/15/155102)

IOP PUBLISHING JOURNAL OF PHYSICS A: MATHEMATICAL AND THEORETICAL

J. Phys. A: Math. Theor. **45** (2012) 155102 (19pp) doi:10.1088/1751-8113/45/15/155102

Inhibitory coherence in a heterogeneous population of subthreshold and suprathreshold type-I neurons

Sang-Yoon Kim[1,4], **Duk-Geun Hong**[1], **Jean Kim**[2] **and Woochang Lim**[3]

[1] Department of Physics, Kangwon National University, Chunchon, Kangwon-Do 200-701, Korea
[2] Wellesley College, Wellesley, MA 02481, USA
[3] Department of Science Education, Daegu National University of Education, Daegu 705-115, Korea

E-mail: sykim@kangwon.ac.kr

Received 24 January 2012, in final form 2 March 2012
Published 27 March 2012
Online at stacks.iop.org/JPhysA/45/155102

Abstract

We study inhibitory coherence (i.e. collective coherence by synaptic inhibition) in a population of globally coupled type-I neurons, which can fire at arbitrarily low frequency. No inhibitory coherence is observed in a homogeneous population composed of only subthreshold neurons, which exhibit noise-induced firings. In addition to subthreshold neurons, there exist spontaneously firing suprathreshold neurons in a noisy environment of a real brain. To take into consideration the effect of suprathreshold neurons on inhibitory coherence, we consider a heterogeneous population of subthreshold and suprathreshold neurons and investigate the inhibitory coherence by increasing the fraction of suprathreshold neurons P_{supra}. As P_{supra} passes a threshold P^*_{supra}, suprathreshold neurons begin to synchronize and play the role of coherent inhibitors for the emergence of inhibitory coherence. Thus, regularly oscillating population-averaged global potential appears for $P_{\text{supra}} > P^*_{\text{supra}}$. For this coherent case, suprathreshold neurons exhibit sparse spike synchronization (i.e. individual potentials of suprathreshold neurons consist of coherent sparse spikings and coherent subthreshold small-amplitude hoppings). By virtue of their coherent inhibition, sparsely synchronized suprathreshold neurons suppress the noisy activity of subthreshold neurons. Thus, subthreshold neurons exhibit hopping synchronization (i.e. only coherent subthreshold hopping oscillations without spikings appear in the individual potentials of subthreshold neurons). We also characterize the inhibitory coherence in terms of the 'statistical-mechanical' spike-based and correlation-based measures, which quantify the average contributions of the microscopic individual spikes and individual potentials

[4] Author to whom any correspondence should be addressed.

to the macroscopic global potential. Finally, the effect of sparse randomness of synaptic connectivity on the inhibitory coherence is briefly discussed.

PACS numbers: 87.19.lm, 87.19.lc

(Some figures may appear in colour only in the online journal)

1. Introduction

Recently, much attention has been paid to rhythms of the brain [1]. Coherence of neural oscillations may be used for efficient sensory and cognitive processing (e.g. feature integration, selective attention, working memory and decision making) [2, 3]. This kind of neural coherence is also correlated with pathological rhythms associated with neural diseases (e.g. epileptic seizures and tremors in the Parkinson disease) [4]. Here, we are interested in these coherent brain rhythms. A brain circuit is composed of a few types of excitatory principal cells and diverse types of inhibitory interneurons. Interneuron diversity increases the computational power of principal cells [1]. The effect of chemical synapses on coherent brain rhythms has much been investigated in neural systems composed of excitatory and/or inhibitory neurons [2, 5]. Historically, recurrent excitation between principal cells is the conventional coherence mechanism [6]. However, when the decay time of the synaptic interaction is enough long, mutual inhibition between interneurons (rather than excitation) may synchronize individual neural firings [7, 8]. By providing a coherent oscillatory output to the principal cells, interneuronal networks play the role of the backbones (i.e. pacemakers) of many brain rhythms, such as the thalamocortical spindle rhythms [9, 10] and the fast gamma rhythms in the hippocampus and the neocortex [11–14]. When the feedback between the excitatory and the inhibitory populations is strong, neural coherence occurs via the 'cross-talk' between the two populations [13–16]. In these computational studies of neural coherence, different types of network architectures have been considered [2]: all-to-all networks, where every neuron is coupled to every other neuron, sparse random networks, where synaptic connections are sparse, and complex networks, such as small-world networks (with predominantly local connections and rare long-distance connections) [17], scale-free networks (with a few percent of hub neurons with an exceptionally large number of connections) [18], and a new type of networks of subnetworks [19].

Neurons in the nervous system exhibit a variety of morphological and physiological properties. However, close to threshold, this remarkable richness may be grouped broadly into two basic types of excitability, often referred to as type I and type II [20]. When the strength of a constant input current passes a threshold, type-I neurons can fire at arbitrarily low frequency and they can smoothly encode the strength of the input into the output firing frequency. In contrast, type-II neurons have a nonzero minimum frequency of firing and they fire in a narrow frequency band, which is relatively insensitive to changes in the strength of the applied current. Different types of excitability occur because neurons have different bifurcations of resting and spiking states [21]. For the type-I neurons, oscillations emerge via a saddle-node bifurcation on an invariant circle. As the bifurcation parameter (i.e. strength of the injected current) passes a threshold, the stable and the unstable fixed points coalesce and then disappear, leaving a large-amplitude stable periodic orbit. Then, the frequency of the global loop can be arbitrarily small. On the other hand, for type-II neurons, a transition from a resting state to a periodically spiking state occurs through Hopf bifurcations with a finite nonzero firing frequency. According to their bifurcations, neurons may also be classified into integrators and resonators [22]. Type-I neurons act as integrators without subthreshold

oscillations, and they prefer high-frequency input: the higher the frequency of the input, the sooner they fire. In contrast, type-II neurons exhibit damped subthreshold oscillations and act as resonators: they prefer oscillatory input with the same frequency as that of damped oscillations. According to their excitability type, neurons make distinctly different responses to stimuli, which have important implications for their distinct roles in generating population rhythms [23–27].

In this paper, we study inhibitory coherence (i.e. collective coherence by synaptic inhibition) in a population of globally coupled type-I neurons. Neural models exhibiting the type-1 excitability include the Connor model for the crab leg axons [28], the Wang–Buzsaki model for inhibitory interneurons [11], the Hindmarsh–Rose model [29] and the Morris–Lecar (ML) model [30] under some circumstances. Among these type-I models, we choose the ML neuron model for our study because it is not only biologically plausible, but also computationally efficient. In section 2, we describe the biological conductance-based ML neuron model with voltage-gated ion channels. The ML neurons (used in our study) exhibit the type-I excitability, and they interact via inhibitory GABAergic synapses whose activity increases quickly and decays slowly. Inhibitory coherence (which is our main concern) is particularly important because it plays a significant role in integration of sensory and cognitive information; for example, impaired inhibitory coherence is believed to be associated with schizophrenia and attention-deficit disorder [31–33]. Hence, it is important to understand mechanisms for the emergence of inhibitory coherence. Many works exploring mechanisms of neural coherence were done in neural systems composed of spontaneously firing (i.e. self-oscillating) suprathreshold neurons (above the threshold) [2, 5]. For this case, neural coherence occurs via cooperation of regular firings of suprathreshold neurons. In addition to suprathreshold neurons, there exist subthreshold neurons below the threshold. These subthreshold neurons exhibit noise-induced firings. Collective coherence between noise-induced spikes of subthreshold neurons has been found to occur as follows. Stochastic excitatory coherence (i.e. collective coherence between noise-induced spikes by synaptic excitation) was observed in a population of excitatory subthreshold neurons [34, 35]. Due to the stochastic excitatory coherence, synaptic current, injected into each individual neuron, becomes temporally coherent. Hence, temporal coherence resonance of an individual subthreshold neuron in the network may be enhanced. Furthermore, stochastic inhibitory coherence (i.e. collective coherence between noise-induced spikes by synaptic inhibition) was also investigated in a population of inhibitory subthreshold ML neurons exhibiting the type-II excitability [36]. Weak stochastic inhibitory coherence was thus found to appear via cooperation of individual irregular oscillations (i.e. a regular small-amplitude population-averaged oscillation emerges from sparsely synchronized neurons discharging irregularly at lower rates than the network oscillation). These sparsely synchronized neural oscillations have been intensively investigated in other types of neural networks [2, 37] and they are believed to be associated with cortical rhythms in cognition (e.g. ultrafast rhythm (100–200 Hz), gamma rhythm (30–100 Hz) and beta rhythm (15–30 Hz)) with irregular and sparse neural discharges (e.g. refer to figure 11 in [2]).

Here, we are interested in the emergence of sparse spike synchronization in an inhibitory population of type-I neurons. In contrast to the case of inhibitory subthreshold type-II ML neurons exhibiting stochastic inhibitory coherence [36], no stochastic inhibitory coherence is observed in an inhibitory population of subthreshold type-I ML neurons. Hence, subthreshold type-I integrator neurons without subthreshold oscillations seem to be much more difficult to synchronize by inhibition than subthreshold type-II resonator neurons exhibiting subthreshold oscillations. As mentioned above, both the subthreshold and the suprathreshold neurons coexist in a noisy environment of a real brain. To take into consideration the effect of

spontaneously firing suprathreshold neurons on the inhibitory coherence, in section 2, we consider a heterogeneous inhibitory population of subthreshold and suprathreshold type-I ML neurons. In section 3, we investigate inhibitory coherence by increasing the fraction of suprathreshold neurons $P_{\rm supra}$ in the whole population. As $P_{\rm supra}$ passes a threshold value $P^*_{\rm supra}$, suprathreshold neurons begin to synchronize and they play the role of coherent inhibitors for the emergence of inhibitory coherence in the whole heterogeneous population. Thus, for $P_{\rm supra} > P^*_{\rm supra}$, the population-averaged global potential V_G exhibits a regular small-amplitude oscillation. For this coherent case, individual suprathreshold neurons exhibit sparse spikings phase-locked to V_G at random multiples of the period of V_G. Due to the stochastic spike skipping of suprathreshold neurons, the interspike interval (ISI) histogram has multiple peaks and partial occupation occurs in the raster plot of neural spikes. In addition to the coherent sparse spikings, coherent subthreshold small-amplitude hopping oscillations also appear in the individual potentials of suprathreshold neurons. In this way, suprathreshold neurons exhibit sparse spike synchronization as in the case of inhibitory subthreshold type-II ML neurons [36]. By virtue of their coherent inhibition, sparsely synchronized suprathreshold neurons suppress noisy activity of subthreshold neurons. Thus, subthreshold neurons exhibit hopping synchronization (i.e. only coherent fast subthreshold hopping oscillations without spikings appear in the individual potentials of subthreshold neurons). We also characterize the inhibitory coherence in terms of 'statistical-mechanical' spike-based [36] and correlation-based [38] measures, which quantify the average contributions of the microscopic individual spikes and individual potentials to the macroscopic population-averaged global potential. Thus, sparse spike synchronization of suprathreshold neurons and hopping synchronization of subthreshold neurons are well characterized in terms of the spike-based and the correlation-based coherence measures, respectively. In a real brain, each neuron is coupled to only a certain number of neurons, which is much smaller than the total number of neurons. The effect of sparseness of synaptic connectivity on the inhibitory coherence is briefly discussed by varying the average number of synaptic inputs per neuron $M_{\rm syn}$ in a random network. The emergence of inhibitory coherence is thus found to persist until $M_{\rm syn}$ is larger than a threshold value $M^*_{\rm syn}$. This kind of inhibitory coherence emerging from sparsely synchronized oscillations of suprathrehold neurons might be associated with cortical rhythms with stochastic and sparse neural discharges, which contribute to cognitive functions in the cerebral cortex (e.g., information integration, working memory and selective attention) [2, 37]. Finally, a summary is given in section 4.

2. Heterogeneous population of inhibitory subthreshold and suprathreshold type-I ML neurons

In this section, we describe the biological neuron model used in our computational study. Both the subthreshold and the suprathreshold neurons coexist in a noisy environment of a real brain. Hence, we consider a heterogeneous inhibitory population of N globally coupled subthreshold and suprathreshold type-I neurons in the presence of noise. As an element in our neural system, we choose the conductance-based ML neuron model, originally proposed to describe the time-evolution pattern of the membrane potential for the giant muscle fibers of barnacles [30]. The population dynamics in this neural network are governed by the following set of stochastic differential equations:

$$C\frac{{\rm d}v_i}{{\rm d}t} = -I_{{\rm ion},i} + I_{{\rm dc},i} + D\xi_i - I_{{\rm syn},i}, \tag{1a}$$

$$\frac{{\rm d}w_i}{{\rm d}t} = \phi\frac{(w_\infty(v_i) - w_i)}{\tau_R(v_i)}, \tag{1b}$$

$$\frac{ds_i}{dt} = \alpha s_\infty(v_i)(1 - s_i) - \beta s_i, \quad i = 1, \ldots, N, \tag{1c}$$

where

$$I_{\text{ion},i} = I_{\text{Ca},i} + I_{K,i} + I_{L,i} \tag{2a}$$

$$= g_{\text{Ca}} m_\infty(v_i)(v_i - V_{\text{Ca}}) + g_K w_i(v_i - V_K) + g_L(v_i - V_L), \tag{2b}$$

$$I_{\text{syn},i} = \frac{J}{N-1} \sum_{j \neq i} s_j(t)(v_i - V_{\text{syn}}), \tag{2c}$$

$$m_\infty(v) = 0.5\,[1 + \tanh\{(v - V_1)/V_2\}]\,, \tag{2d}$$

$$w_\infty(v) = 0.5\,[1 + \tanh\{(v - V_3)/V_4\}]\,, \tag{2e}$$

$$\tau_R(v) = 1/\cosh\{(v - V_3)/(2V_4)\}\,, \tag{2f}$$

$$s_\infty(v_i) = 1/[1 + \mathrm{e}^{-(v_i - v_t)/\delta}]. \tag{2g}$$

Here, the state of the ith neuron at a time t (measured in units of ms) is characterized by three state variables: the membrane potential v_i (measured in units of mV), the slow recovery variable w_i representing the activation of the K^+ current (i.e. the fraction of open K^+ channels) and the synaptic gating variable s_i denoting the fraction of open synaptic ion channels. In equation (1*a*), C represents the capacitance of the membrane of each neuron, and the time evolution of v_i is governed by four kinds of source currents.

The total ionic current $I_{\text{ion},i}$ of the ith neuron consists of the calcium current $I_{\text{Ca},i}$, the potassium current $I_{K,i}$ and the leakage current $I_{L,i}$. Each ionic current obeys Ohm's law. The constants g_{Ca}, g_K and g_L are the maximum conductances for the ion and the leakage channels, and the constants V_{Ca}, V_K and V_L are the reversal potentials at which each current is balanced by the ionic concentration difference across the membrane. Since the calcium current $I_{\text{Ca},i}$ changes much faster than the potassium current $I_{K,i}$, the gate variable m_i for the Ca^{2+} channel is assumed to always take its saturation value $m_\infty(v_i)$. On the other hand, the activation variable w_i for the K^+ channel approaches its saturation value $w_\infty(v_i)$ with a relaxation time $\tau_R(v_i)/\phi$, where τ_R has a dimension of ms and ϕ is a (dimensionless) temperature-like time scale factor.

Each ML neuron is also stimulated by a dc current $I_{\text{dc},i}$ and a Gaussian white noise ξ_i (see the second and third terms in equation (1*a*)) satisfying $\langle \xi_i(t) \rangle = 0$ and $\langle \xi_i(t)\xi_j(t') \rangle = \delta_{ij}\delta(t - t')$, where $\langle \cdots \rangle$ denotes the ensemble average. The noise ξ_i is a parametric one which randomly perturbs the strength of the applied current $I_{\text{dc},i}$, and its intensity is controlled by the parameter D. Depending on the system parameters, the ML neuron may exhibit either type-I or type-II excitability [21]. Throughout this paper, we consider the case of type-I excitability, where $g_{\text{Ca}} = 4$ mS cm^{-2}, $g_K = 8$ mS cm^{-2}, $g_L = 2$ mS cm^{-2}, $V_{\text{Ca}} = 120$ mV, $V_K = -84$ mV, $V_L = -60$ mV, $C = 20$ μF cm^{-2}, $\phi = 1/15$, $V_1 = -1.2$ mV, $V_2 = 18$ mV, $V_3 = 12$ mV and $V_4 = 17.4$ mV. Only for comparison, a result on the order parameter is given in figure 1(*c*) for the type-II case, where the values of the above parameters are the same as those in the type-I case except that $g_{\text{Ca}} = 4.4$ mS cm^{-2}, $\phi = 0.04$, $V_3 = 2$ mV and $V_4 = 30$ mV. For the type-I case, a transition from a resting state to a spiking state occurs for $I^*_{\text{dc}} \simeq 40$ μA cm^{-2} via a saddle-node bifurcation on an invariant circle [21], and firing begins at arbitrarily low frequency. On the other hand, a type-II neuron exhibits a jump from a resting state to a spiking state through a subcritical Hopf bifurcation for $I^*_{\text{dc},h} \simeq 93.9$ μA cm^{-2} by absorbing an unstable limit cycle born via fold limit cycle bifurcation

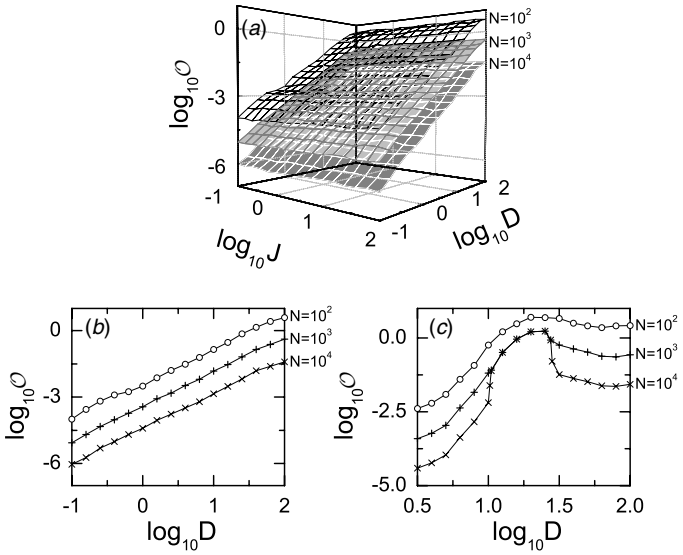

Figure 1. Plots of the order parameter $\mathcal{O}$ versus (a) both the coupling strength J and the noise intensity D and versus (b) D for $J = 20$ mS cm^{-2} in N globally coupled inhibitory subthreshold type-I ML neurons. The value of $I_{\mathrm{dc},i}$ for each subthreshold type-I neuron is randomly chosen with a uniform probability in the range of $(I^*_{\mathrm{dc}} - \Delta, I^*_{\mathrm{dc}})$, where $I^*_{\mathrm{dc}} = 40\ \mu$A cm^{-2} and $\Delta = 10\ \mu$A cm^{-2}. (c) Plots of $\mathcal{O}$ versus D for $J = 3$ mS cm^{-2} in N globally coupled inhibitory subthreshold type-II ML neurons. The value of $I_{\mathrm{dc},i}$ for each subthreshold type-II neuron is randomly chosen with a uniform probability in the range of $(I^*_{\mathrm{dc},l} - \Delta, I^*_{\mathrm{dc},l})$, where $I^*_{\mathrm{dc},l} = 88.3\ \mu$A cm^{-2} and $\Delta = 10\ \mu$A cm^{-2}.

for $I^*_{\mathrm{dc},l} \simeq 88.3\ \mu$A cm^{-2} [21], and hence, the firing frequency begins from a nonzero value. Here, a spread in the value of the dc input current I_{dc} is taken into consideration. For the type-I case, the values of $I_{\mathrm{dc},i}$ for the subthreshold and the suprathreshold neurons are randomly chosen with a uniform probability in the range of $(I^*_{\mathrm{dc}} - \Delta, I^*_{\mathrm{dc}})$ and $(I^*_{\mathrm{dc}}, I^*_{\mathrm{dc}} + \Delta)$, respectively, where the spread parameter Δ is set as $\Delta = 10\ \mu$A cm^{-2}.

We consider a heterogeneous inhibitory population of N globally coupled subthreshold and suprathreshold ML neurons where the fraction of suprathreshold neurons is given by $P_{\mathrm{supra}} = \frac{N_{\mathrm{supra}}}{N}$ (N_{supra}: number of suprathreshold neurons). The last term in equation (1a) represents the synaptic coupling between neurons in the network. Each neuron is connected to all the other ones through global synaptic couplings. $I_{\mathrm{syn},i}$ of equation (2c) represents such synaptic current injected into the ith neuron. Here, the coupling strength is controlled by the parameter J and V_{syn} is the synaptic reversal potential. We use $V_{\mathrm{syn}} = -80$ mV for the inhibitory synapse. The synaptic gating variable s obeys the first-order kinetics of equation (1c) [10, 11]. Here, the normalized concentration of neurotransmitters $s_\infty(v)$, activating the synapse, is assumed to be an instantaneous sigmoidal function of the membrane potential with a threshold v_t in equation (2g), where we set $v_t = 0$ mV and $\delta = 2$ mV. For the inhibitory GABAergic synapse (involving the $\mathrm{GABA_A}$ receptors), the synaptic channel opening rate, corresponding to the inverse of the synaptic rise time τ_r, is $\alpha = 10\ \mathrm{ms}^{-1}$, and the synaptic closing rate β, which is the inverse of the synaptic decay time τ_d, is $\beta = 0.1\ \mathrm{ms}^{-1}$ [11, 16]. Hence, I_{syn} rises fast and decays slowly.

Numerical integration of equation (1a) is done using the Heun method for the stochastic differential equation [39] (with the time step $\Delta t = 0.01$ ms), and data for (v_i, w_i, s_i)

($i = 1, \ldots, N$) are obtained with the sampling time interval $\Delta t = 1$ ms. For each realization of the stochastic process in equation (1), we choose a random initial point $[v_i(0), w_i(0), s_i(0)]$ for the ith ($i = 1, \ldots, N$) neuron with uniform probability in the range of $v_i(0) \in (-70, 50)$, $w_i(0) \in (0.0, 0.6)$ and $s_i(0) \in (0.0, 1.0)$.

3. Inhibitory coherence emerging from sparsely synchronized oscillations of suprathreshold neurons

In this section, we are concerned about inhibitory coherence in a heterogeneous population of N globally coupled subthreshold and suprathreshold type-I ML neurons in the presence of noise. By increasing the fraction of suprathreshold neurons P_{supra}, we investigate inhibitory coherence that emerges from sparsely synchronized oscillations of suprathreshold neurons. Hereafter, for convenience, we omit the dimensions of I_{dc}, D and J.

We first consider a homogeneous population (corresponding to the case of $P_{\text{supra}} = 0$) composed of only subthreshold type-I ML neurons and study the inhibitory coherence by varying both the coupling strength J and the noise intensity D. The emergence of inhibitory coherence may be well described by the population-averaged global potential

$$V_G(t) = \frac{1}{N} \sum_{i=1}^{N} v_i(t). \tag{3}$$

In the thermodynamic limit ($N \to \infty$), a collective state becomes coherent if $\Delta V_G(t)$ ($= V_G(t) - \overline{V_G(t)}$) is non-stationary (i.e. an oscillating global potential V_G appears for a coherent case), where the overbar represents the time average. Otherwise (i.e. when ΔV_G is stationary), it becomes incoherent. Thus, the mean-square deviation of the global potential V_G (i.e. time-averaged fluctuations of V_G),

$$\mathcal{O} \equiv \overline{(V_G(t) - \overline{V_G(t)})^2}, \tag{4}$$

plays the role of an order parameter used for describing the coherence–incoherence transition [40]. For the coherent (incoherent) state, the order parameter $\mathcal{O}$ approaches a nonzero (zero) limit value as N tends to the infinity. Figure 1(a) shows plots of the order parameter versus both the coupling strength J and the noise intensity D. As N is increased, the order parameter tends to decrease, independent of J and D. An example of the order parameter is shown in figure 1(b) for $J = 20$. For any given D, $\mathcal{O}$ tends to zero as N is increased. Hence, only incoherent states exist, irrespective of D. This is in contrast to the case of subthreshold type-II neurons exhibiting inhibitory coherence [36]. Figure 1(c) shows plots of the order parameter versus the noise intensity for the type-II case of $J = 3$. Unlike the type-I case, coherent states exist in an intermediate range of noise intensity ($D_l^* (\simeq 10.3) < D < D_h^* (\simeq 27.9)$), where the order parameter approaches a nonzero limit value as N increases. Hence, subthreshold type-I neurons (used in our study) seem to be much more difficult to synchronize by synaptic inhibition than subthreshold type-II neurons.

In addition to subthreshold neurons, spontaneously firing suprathreshold neurons also exist in a noisy environment of a real brain. To take into consideration the effect of suprathreshold neurons on the inhibitory coherence, we consider a heterogeneous population consisting of subthreshold and suprathreshold type-I ML neurons for $J = 20$. For convenience, we set the value of noise intensity as $D = 8$ and investigate the inhibitory coherence by increasing the fraction of suprathreshold neurons P_{supra}. Figure 2($a1$) shows the plots of the order parameter

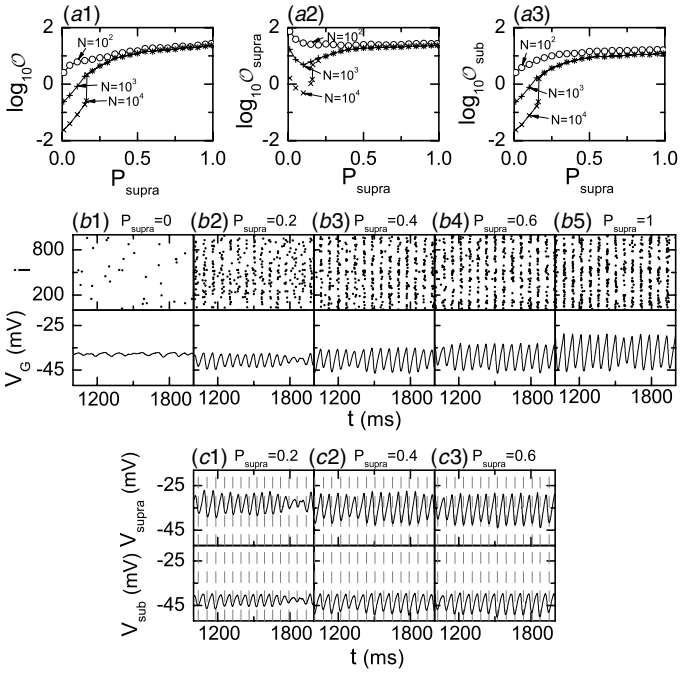

Figure 2. Order parameters, raster plots of neural spikes and time series of global potentials in the heterogeneous ensemble of N globally coupled inhibitory type-I ML neurons for $J = 20$ mS cm^{-2} and $D = 8$ μA ms$^{1/2}$ cm^{-2}; $N = 10^3$ in ($b1$)–($b5$) and ($c1$)–($c3$). The value of $I_{\mathrm{dc},i}$ for each subthreshold (suprathreshold) type-I ML neuron is randomly chosen with a uniform probability in the range of $(I^*_{\mathrm{dc}} - \Delta, I^*_{\mathrm{dc}})$ $((I^*_{\mathrm{dc}}, I^*_{\mathrm{dc}} + \Delta))$, where $I^*_{\mathrm{dc}} = 40$ μA cm^{-2} and $\Delta = 10$ μA cm^{-2}. Plots of the order parameter $\mathcal{O}$ versus the fraction of suprathreshold neurons P_{supra} in ($a1$) the whole population and in the two subpopulations of ($a2$) the suprathreshold and ($a3$) the subthreshold neurons. Raster plots and time series of the global potential V_G in the whole population for $P_{\mathrm{supra}} =$ 0, 0.2, 0.4, 0.6 and 1.0 in ($b1$)–($b5$). Time series of the subpopulation-averaged potentials V_{supra} and V_{sub} in the two subpopulations of the suprathreshold and the subthreshold neurons for $P_{\mathrm{supra}} =$ 0.2, 0.4 and 0.6 in ($c1$)–($c3$). Vertical dashed lines in ($c1$)–($c3$) represent the times at which the local minima of V_G appear.

$\mathcal{O}$ versus P_{supra} in the whole population. As P_{supra} passes a threshold value $P^*_{\mathrm{supra}}(\simeq 0.16)$, a transition from an incoherent state to a coherent state occurs. As shown in figure 2($a1$), it is enough to consider only the case of $N = 10^3$ for the study of inhibitory coherence because the values of the order parameter $\mathcal{O}$ for the coherent states become saturated for $N = 10^3$. Hence, we set the number of neurons as $N = 10^3$ in all cases except the calculation of the order parameter. For an incoherent case of $P_{\mathrm{supra}} = 0$, the raster plot consists of randomly scattered sparse spikes and the global potential V_G exhibits a nearly stationary irregular oscillation (see figure 2($b1$)); the amplitude of V_G decreases with further increase in N. However, when passing the threshold P^*_{supra}, partially occupied 'stripes' (composed of spikes and indicating collective coherence) appear in the raster plot together with regularly oscillating small-amplitude V_G with frequency f_G (= 13.8 Hz) (see figure 2($b2$) for $P_{\mathrm{supra}} = 0.2$). As P_{supra} is further increased, both the pacing degree of spikes in the raster plot and the amplitude of V_G (representing the degree of collective coherence) increase, as shown in figures 2($b3$)–($b5$), where $f_G = 14.3$, 13.6 and 14.2 Hz. This kind of weak inhibitory coherence also occurs in each subpopulation of the subthreshold and the suprathreshold neurons. As in the case of the whole population,

the emergence of inhibitory coherence in the subpopulations may be well described by the subpopulation-averaged potentials $V_{\rm supra}$ and $V_{\rm sub}$:

$$V_{\rm supra}(t) = \frac{1}{N_{\rm supra}} \sum_{i=1}^{N_{\rm supra}} v_i(t), \qquad V_{\rm sub}(t) = \frac{1}{N_{\rm sub}} \sum_{i=1}^{N_{\rm sub}} v_i(t), \tag{5}$$

where $N_{\rm supra}$ ($N_{\rm sub}$) is the number of suprathreshold (subthreshold) neurons. Then, the order parameters $\mathcal{O}_{\rm supra}$ and $\mathcal{O}_{\rm sub}$, defined by the mean-square deviation of $V_{\rm supra}$ and $V_{\rm sub}$,

$$\mathcal{O}_{\rm supra} \equiv \overline{(V_{\rm supra}(t) - \overline{V_{\rm supra}(t)})^2}, \quad \mathcal{O}_{\rm sub} \equiv \overline{(V_{\rm sub}(t) - \overline{V_{\rm sub}(t)})^2}, \tag{6}$$

may be used for describing the coherence–incoherence transitions in the subpopulations of suprathreshold and subthreshold neurons, respectively. The plots of $\mathcal{O}_{\rm supra}$ and $\mathcal{O}_{\rm sub}$ versus $P_{\rm supra}$ are shown in figures 2(*a*2) and (*a*3), respectively. We note that the coherent transition in each subpopulation occurs at the same threshold value $P^*_{\rm supra}(\simeq 0.16)$. For the case of coherent states, not only $V_{\rm supra}$ but also $V_{\rm sub}$ exhibits regular oscillations whose amplitudes increase as $P_{\rm supra}$ is increased (see figures 2(*c*1)–(*c*3), where vertical dashed lines in $V_{\rm supra}$ and $V_{\rm sub}$ denote the times at which local minima of V_G appear). Both $V_{\rm supra}$ and $V_{\rm sub}$ are phase-locked to V_G.

To further understand the emergence of inhibitory coherence, we examine the individual and the global output signals in the subpopulations of subthreshold and suprathreshold neurons. We first consider the subpopulation of suprathreshold neurons. As explained in section 2, the values of $I_{{\rm dc},i}$ for the suprathreshold neurons are randomly chosen with a uniform probability in the range of $(I^*_{\rm dc}, I^*_{\rm dc} + \Delta)$, where the spread parameter Δ is set as $\Delta = 10$. Then, the intrinsic frequencies of suprathreshold neurons (in the absence of noise and coupling) are distributed in a range of (0, 13.2) Hz, and the average value and the standard deviation from the mean value for the distribution of intrinsic frequencies are 9.4 and 2.9 Hz, respectively [21]. Figures 3(*a*1)–(*a*5) show the time series of the individual potential v_1 of the first neuron and the time series of the global potential $V_{\rm supra}$ in the subpopulation of the suprathreshold neurons. For an incoherent case, $V_{\rm supra}$ shows a nearly stationary irregular oscillation and only stochastic intermittent spikings occur without any coherent hoppings in the individual potential of suprathreshold neurons, as shown in figure 3(*a*1) for $P_{\rm supra} = 0.1$. However, when passing the threshold $P^*_{\rm supra}$ ($\simeq 0.16$), a coherent transition occurs, and then, $V_{\rm supra}$ exhibits regular small-amplitude oscillations (see figures 3(*a*2)–(*a*5)). For this coherent case, individual suprathreshold neurons exhibit sparse spikings phase-locked to $V_{\rm supra}$ at random multiples of the period of $V_{\rm supra}$ (see figures 3(*a*2)–(*a*5) where dashed lines denote the times at which the local minima of $V_{\rm supra}$ appear). This 'stochastic phase locking' leading to stochastic spike skipping is well shown in the ISI histogram with multiple peaks (see figures 3(*d*2)–(*d*5)), which will be explained below in details. In addition to these coherent sparse spiking phases, coherent subthreshold small-amplitude hopping oscillations also appear in the individual potentials of suprathreshold neurons. In this way, suprathreshold neurons exhibit sparse spike synchronization. That is, they exhibit sparsely synchronized oscillations with two well-separated frequency scales, a fast subthreshold hopping frequency f_h imposed by the collective network oscillation with the frequency f_G ($\simeq$ 14 Hz) and a lower spiking frequency f_s of individual suprathreshold neurons: $f_s = 3.6$, 2.8, 2.3 and 1.8 Hz, in figures 3(*a*2)–(*a*5), respectively. For the case of the GABAergic synapse (we use in our study), gamma network oscillations with frequency in the range of (30, 100) Hz occur usually in a population of inhibitory neurons with fast intrinsic frequencies (e.g., 55–63 Hz in figure 8(A) in [11]). However, since suprathreshold neurons for our case have slow intrinsic frequencies in a range of (0, 13.2) Hz, the network oscillation frequency f_G ($\simeq$ 14) Hz seems to become less than the gamma frequency. These sparsely synchronized suprathreshold neurons play the role of coherent inhibitors for the emergence of inhibitory coherence in the whole heterogeneous population, as shown below.

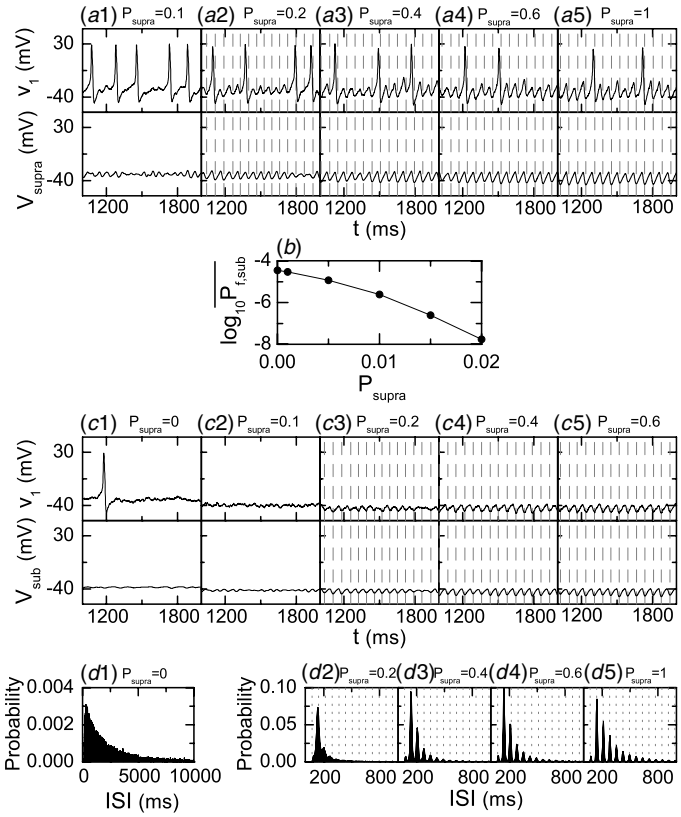

Figure 3. Time series of the individual and the global potentials, the average firing probability and the ISI histogram in the heterogeneous ensemble of $N(=10^3)$ globally coupled inhibitory type-I ML neurons for $J = 20$ mS cm^{-2} and $D = 8$ μA ms$^{1/2}$ cm^{-2}. The value of $I_{\mathrm{dc},i}$ for each subthreshold (suprathreshold) type-I ML neuron is randomly chosen with a uniform probability in the range of $(I^*_{\mathrm{dc}} - \Delta, I^*_{\mathrm{dc}})$ $((I^*_{\mathrm{dc}}, I^*_{\mathrm{dc}} + \Delta))$, where $I^*_{\mathrm{dc}} = 40$ μA cm^{-2} and $\Delta = 10$ μA cm^{-2}. The individual potential v_1 of the first neuron and the global potential V_{supra} in the subpopulation of suprathreshold neurons for $P_{\mathrm{supra}} = 0.1$, 0.2, 0.4, 0.6 and 1.0 in (a1)–(a5). Vertical dashed lines in (a2)–(a5) represent the times at which the local minima of V_{supra} appear. (b) The plot of the average firing probability $\overline{P_{f,\mathrm{sub}}}$ versus the fraction of suprathreshold neurons P_{supra}. The individual potential v_1 of the first neuron and the global potential V_{sub} in the subpopulation of subthreshold neurons for $P_{\mathrm{supra}} = 0$, 0.1, 0.2, 0.4 and 0.6 in (c1)–(c5). Vertical dashed lines in (c3)–(c5) denote the times at which the local minima of V_{sub} appear. ISI histograms in the whole population for $P_{\mathrm{supra}} = 0$, 0.2, 0.4, 0.6 and 1.0 in (d1)–(d5); each ISI histogram is composed of 5×10^4 ISIs and the bin size for the histogram is 5 ms. Vertical dotted lines in (d2)–(d5) denote integer multiples of T_G (period of V_G).

We now consider the subpopulation of subthreshold neurons. Figure 3(b) shows the plot of the average firing probability $\overline{P_{f,\mathrm{sub}}}$ versus P_{supra} in the subpopulation of subthreshold neurons (i.e. time-averaged fraction of firing subthreshold neurons in the subpopulation of subthreshold neurons). Due to inhibition, $\overline{P_{f,\mathrm{sub}}}$ decreases dramatically with respect to P_{supra}. For $P_{\mathrm{supra}} > 0.02$, one can disregard spikes of subthreshold neurons because $\overline{P_{f,\mathrm{sub}}}(\sim 10^{-8})$ becomes very small. In contrast to the case of suprathreshold neurons, subthreshold neurons seem to be largely irrelevant for the synaptic inhibition because their spikes may be negligible. Hence, the synaptic current $I_{\mathrm{syn},i}$ of equation (2c) may be well approximated by taking into consideration the synaptic effect of only the suprathreshold neurons. Then, the synaptic

currents injected into the suprathreshold and the subthreshold neurons, i.e., $I_{\mathrm{syn},i}^{(\mathrm{supra})}$ and $I_{\mathrm{syn},i}^{(\mathrm{sub})}$, are given by

$$I_{\mathrm{syn},i}^{(\mathrm{supra})} \simeq \frac{J_{\mathrm{supra}}}{N_{\mathrm{supra}}-1} \sum_{j\neq i} s_j(t)(v_i - V_{\mathrm{syn}}), \tag{7a}$$

$$I_{\mathrm{syn},i}^{(\mathrm{sub})} \simeq \frac{J_{\mathrm{supra}}}{N_{\mathrm{supra}}} \sum_{j}^{N_{\mathrm{supra}}} s_j(t)(v_i - V_{\mathrm{syn}}), \tag{7b}$$

where $J_{\mathrm{supra}} = J P_{\mathrm{supra}}$ ($J = 20$ for our case) and the summations are done only in the suprathreshold subpopulation. The time series of the individual potential v_1 of the first neuron and the time series of the global potential V_{sub} in the subpopulation of the subthreshold neurons are shown in figures 3($c1$)–($c5$). For an incoherent case, V_{sub} exhibits nearly stationary irregular oscillations as shown in figures 3($c1$) and ($c2$) for $P_{\mathrm{supra}} = 0$ and 0.1, respectively. However, as P_{supra} passes a threshold P^*_{supra}, a coherent transition occurs, and then, regular oscillations with a small amplitude appear in V_{sub} (see figures 3($c3$)–($c5$)). For the coherent case, sparsely synchronized suprathreshold neurons suppress the noisy activity of subthreshold neurons by virtue of their coherent inhibition, and then, individual subthreshold neurons exhibit only coherent subthreshold hoppings without spikings. Thus, subthreshold neurons exhibit hopping synchronization, in contrast to sparse spike synchronization of suprathreshold neurons. By taking into consideration the fact that only the suprathreshold neurons are practically relevant for the synaptic inhibition, we understand the coherent transition occurring when passing a threshold P^*_{supra} in the following way. The increase in P_{supra} means the growth of the size of the relevant spiking part for the synaptic inhibition in the whole population. Hence, individual neurons receive more synaptic inhibition as P_{supra} is increased. For this case, the threshold P^*_{supra} in the whole population is associated with the critical value of the coupling strength J^*_{supra} in the incoherence–coherence transition that occurs by varying J_{supra} ($= 20P_{\mathrm{supra}}$) in an inhibitory ensemble composed of only suprathreshold neurons. As J_{supra} passes a threshold J^*_{supra}, suprathreshold neurons begin to exhibit sparse spike synchronization by the synaptic inhibition of equation (7a), and by virtue of their coherent inhibition of equation (7b), subthreshold neurons show hopping synchronization. In this way, inhibitory coherence, which emerges from sparsely synchronized oscillations of suprathreshold neurons, occurs in the whole population. Particularly, sparse spike synchronization exhibited by suprathreshold neurons may be seen well in the ISI histograms. Figures 3($d1$)–($d5$) show the ISI histograms in the whole population. (As shown above, spiking neurons in the whole population are just suprathreshold ones for $P_{\mathrm{supra}} > 0.02$.) The ISI histogram for $P_{\mathrm{supra}} = 0$ has a very long tail, and hence, the average value $\langle \mathrm{ISI} \rangle (\simeq 4926$ ms) of ISIs is very large. As P_{supra} passes the threshold P^*_{supra}, multiple peaks tend to appear at integer multiples of T_G (period of V_G) (i.e. $n\,T_G$ ($n = 1, 2, 3, \ldots$)) (e.g., see the ISI histogram for $P_{\mathrm{supra}} = 0.2$; vertical dotted lines in the histogram denote integer multiples of T_G (=72.4 ms)). As P_{supra} is further increased, ISI histograms with more distinct multiple peaks appear due to the stochastic spike skipping resulting from stochastic phase locking of the suprathreshold neurons, as shown in figures 3($d3$)–($d5$) where $T_G = 69.9$, 73.3 and 70.3 ms, respectively. The most probable peak appears at $2\,T_G$, and hence, suprathreshold neurons fire mostly in alternate global cycles.

We also characterize the inhibitory coherence that emerges from sparsely synchronized oscillations of suprathreshold neuorns in terms of two kinds of 'statistical-mechanical' spike-based [36] and correlation-based [38] measures. These statistical-mechanical measures quantify the average contributions of the microscopic individual spikes and individual potentials to the macroscopic population-averaged global potential V_G. They are in contrast to the 'thermodynamic' order parameter $\mathcal{O}$ of equation (4), which concerns the time-averaged

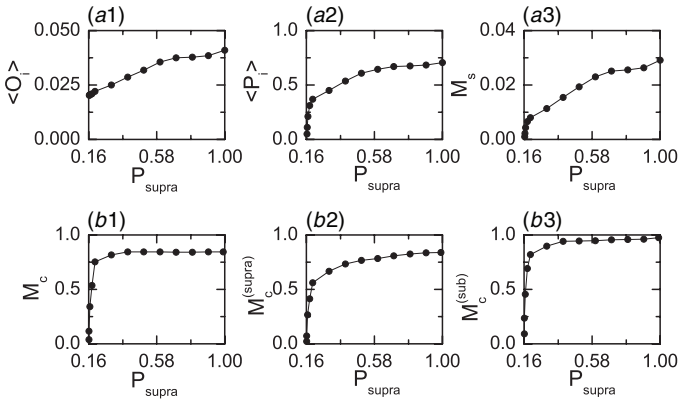

Figure 4. 'Statistical-mechanical' coherence measures in the heterogeneous ensemble of $N(=10^3)$ globally coupled inhibitory type-I ML neurons for $J = 20$ mS cm^{-2} and $D = 8$ μA ms$^{1/2}$ cm^{-2}. (*a*) Spike-based coherence measure M_s: (*a*1) the plot of the average occupation degree $\langle O_i \rangle$ versus the fraction of suprathreshold neurons P_{supra}, (*a*2) the plot of the average pacing degree $\langle P_i \rangle$ versus P_{supra} and (*a*3) the plot of the spiking coherence measure M_s versus P_{supra}. To obtain $\langle O_i \rangle$, $\langle P_i \rangle$ and M_s, we follow the 3×10^3 stripes for each P_{supra}. (*b*) Correlation-based coherence measure M_c: (*b*1) the plot of M_c versus P_{supra} in the whole population and plots of $M_c^{(\text{supra})}$ and $M_c^{(\text{sub})}$ versus P_{supra} in the two subpopulations of (*b*2) suprathreshold and (*b*3) subthreshold neurons. The number of data used for the calculation of a cross-correlation function for each P_{supra} is 2^{12}.

fluctuations of just the macroscopic global potential V_G without considering any quantitative relation between V_G and the microscopic individual potentials. As shown in figures 2(*b*2)–(*b*5), sparse spike synchronization may be well visualized in the raster plot of spikes. For this case, the raster plot is composed of partially occupied stripes (indicating collective coherence). To measure the degree of the sparse spike synchronization shown in the raster plot, a new spike-based measure M_s was introduced by considering the occupation pattern and the pacing pattern of neural spikes in the 'stripes' [36]. Particularly, the pacing degree between spikes is determined in a statistical-mechanical way by quantifying the average contribution of microscopic individual spikes to the global potential V_G. The spiking coherence measure M_i of the ith stripe is defined by the product of the occupation degree O_i of spikes (representing the density of the ith stripe) and the pacing degree P_i of spikes (denoting the smearing of the ith stripe):

$$M_i = O_i \cdot P_i. \tag{8}$$

The occupation degree O_i in the ith stripe is given by the fraction of spiking neurons:

$$O_i = \frac{N_i^{(s)}}{N}, \tag{9}$$

where $N_i^{(s)}$ is the number of spiking neurons in the ith stripe. For the full occupation, $O_i = 1$, while for the partial occupation, $O_i < 1$. The pacing degree P_i of each microscopic spike in the ith stripe can be determined in a statistical-mechanical way by taking into consideration its contribution to the macroscopic global potential V_G. Each global cycle of V_G begins from its left minimum, passes the central maximum and ends at the right minimum; the central maxima coincide with centers of stripes in the raster plot (see figures 2(*b*2)–(*b*5)). An instantaneous global phase $\Phi(t)$ of V_G is introduced via linear interpolation in the two successive subregions forming a global cycle [41] (e.g., refer to figure 4(*b*) in [36]). The global phase $\Phi(t)$ between

the left minimum (corresponding to the beginning point of the ith global cycle) and the central maximum is given by

$$\Phi(t) = 2\pi\,(i - 3/2) + \pi \left(\frac{t - t_i^{(\min)}}{t_i^{(\max)} - t_i^{(\min)}} \right) \quad \text{for } t_i^{(\min)} \leqslant t < t_i^{(\max)} \quad (i = 1, 2, 3, \ldots), \quad (10)$$

and $\Phi(t)$ between the central maximum and the right minimum (corresponding to the beginning point of the $(i + 1)$th cycle) is given by

$$\Phi(t) = 2\pi\,(i - 1) + \pi \left(\frac{t - t_i^{(\max)}}{t_{i+1}^{(\min)} - t_i^{(\max)}} \right) \quad \text{for } t_i^{(\max)} \leqslant t < t_{i+1}^{(\min)} \quad (i = 1, 2, 3, \ldots), \quad (11)$$

where $t_i^{(\min)}$ is the beginning time of the ith global cycle (i.e. the time at which the left minimum of V_G appears in the ith global cycle) and $t_i^{(\max)}$ is the time at which the maximum of V_G appears in the ith global cycle. Then, the contribution of the kth microscopic spike in the ith stripe occurring at the time $t_k^{(s)}$ to V_G is given by $\cos\Phi_k$, where Φ_k is the global phase at the kth spiking time (i.e. $\Phi_k \equiv \Phi(t_k^{(s)})$). A microscopic spike makes the most constructive (in-phase) contribution to V_G when the corresponding global phase Φ_k is $2\pi n$ ($n = 0, 1, 2, \ldots$), while it makes the most destructive (anti-phase) contribution to V_G when Φ_i is $2\pi\,(n - 1/2)$. By averaging the contributions of all microscopic spikes in the ith stripe to V_G, we obtain the pacing degree of spikes in the ith stripe:

$$P_i = \frac{1}{S_i} \sum_{k=1}^{S_i} \cos\Phi_k, \quad (12)$$

where S_i is the total number of microscopic spikes in the ith stripe. By averaging M_i given in equation (8) over a sufficiently large number N_s of stripes, we obtain the spike-based coherence measure M_s:

$$M_s = \frac{1}{N_s} \sum_{i=1}^{N_s} M_i. \quad (13)$$

By varying P_{supra}, we follow 3×10^3 stripes and measure the degree of collective spiking coherence in terms of $\langle O_i \rangle$ (average occupation degree), $\langle P_i \rangle$ (average pacing degree) and M_s for 13 values of P_{supra} in the coherent regime, and the results are shown in figures 4(a1)–(a3). As P_{supra} is increased, the average occupation degree $\langle O_i \rangle$ (denoting the average density of stripes in the raster plot) increases slowly, but its values are very small ($\langle O_i \rangle < 0.05$); only a fraction (less than 1/20) of the total neurons in the whole population fire in each stripe (see figures 2(b2)–(b5)). This partial occupation results from stochastic spike skipping of suprathreshold neurons shown well in the multi-peaked ISI histograms (see figures 3(d2)–(d5)). On the other hand, the average pacing degree $\langle P_i \rangle$ increases rapidly near the threshold P^*_{supra}, and then, it grows slowly. This tendency may be understood from the change in the structure of the ISI histograms. As P_{supra} is increased, clear well-separated multiple peaks appear, and hence, the average pacing degree of the stripes becomes better with increasing P_{supra}. In most of the coherent region, the values of $\langle P_i \rangle$ are large in contrast to $\langle O_i \rangle$. However, the spiking measure M_s of equation (13) (representing the degree of collective spiking coherence) is very low due to the partial occupation in the raster plot. We note that this spike-based coherence measure M_s represents the degree of sparse spike synchronization of suprathreshold neurons in the whole population very well.

Unlike the suprathreshold neurons, subthreshold neurons exhibit only coherent subthreshold hoppings without spikings. Hence, they make no contribution to the spike-based measure M_s. To measure the degree of hopping synchronization exhibited by subthreshold

neurons, we use another statistical-mechanical measure based on the ensemble average of cross-correlations between the macroscopic global potential V_G and the microscopic individual potentials v_i [38]. The inhibitory coherence in the whole population is quantified in terms of the coherence measure M_c given by the ensemble average of the global-individual cross-correlations $C_i(0)$ between V_G and v_i at the zero-time lag:

$$M_c = \frac{1}{N}\sum_{i=1}^{N} C_i(0). \tag{14}$$

Here, the normalized cross-correlation function $C_i(\tau)$ between V_G and v_i is given by

$$C_i(\tau) = \frac{\overline{\Delta V_G(t+\tau)\,\Delta v_i(t)}}{\sqrt{\overline{\Delta V_G^2(t)}}\sqrt{\overline{\Delta v_i^2(t)}}}, \tag{15}$$

where τ is the time lag, $\Delta V_G(t) = V_G(t) - \overline{V_G(t)}$, $\Delta v_i(t) = v_i(t) - \overline{v_i(t)}$ and the overline denotes the time average. As mentioned above, this correlation-based measure M_c can be regarded as a 'statistical-mechanical' measure because it quantifies the average contributions of the microscopic individual potentials to the macroscopic global potential. Hence, M_c is in contrast to the conventional microscopic measure based on the cross-correlations between the microscopic individual potentials. As in the case of the whole population, the degree of inhibitory coherence in each subpopulation of the subthreshold and the suprathreshold neurons may be well quantified in terms of the coherence measures $M_c^{(\mathrm{sub})}$ and $M_c^{(\mathrm{supra})}$ based on the cross-correlations between the global potentials (V_{sub} and V_{supra}) and the individual potentials v_i:

$$M_c^{(\mathrm{supra})} = \frac{1}{N_{\mathrm{supra}}}\sum_{i=1}^{N_{\mathrm{supra}}} C_i^{(\mathrm{supra})}(0), \quad M_c^{(\mathrm{sub})} = \frac{1}{N_{\mathrm{sub}}}\sum_{i=1}^{N_{\mathrm{sub}}} C_i^{(\mathrm{sub})}(0), \tag{16}$$

where

$$C_i^{\mathrm{supra}}(\tau) = \frac{\overline{\Delta V_{\mathrm{supra}}(t+\tau)\,\Delta v_i(t)}}{\sqrt{\overline{\Delta V_{\mathrm{supra}}^2(t)}}\sqrt{\overline{\Delta v_i^2(t)}}}\ (i = 1, ..., N_{\mathrm{supra}}), \tag{17}$$

$$C_i^{\mathrm{sub}}(\tau) = \frac{\overline{\Delta V_{\mathrm{sub}}(t+\tau)\,\Delta v_i(t)}}{\sqrt{\overline{\Delta V_{\mathrm{sub}}^2(t)}}\sqrt{\overline{\Delta v_i^2(t)}}}\ (i = 1, ..., N_{\mathrm{sub}}). \tag{18}$$

By varying P_{supra}, we measure the degree of inhibitory coherence in terms of the correlation-based measures M_c, $M_c^{(\mathrm{supra})}$ and $M_c^{(\mathrm{sub})}$ not only in the whole population, but also in the subpopulations of the subthreshold and the suprathreshold neurons, and the results are shown in figures 4(*b*1)–(*b*3). All of the coherence measures increase rapidly near the threshold P_{supra}^*, and then, they grow slowly. The values of these correlation-based measures are very large in contrast to the spiking coherence measure M_s. We also note that the degree of hopping synchronization $M_c^{(\mathrm{sub})}$ in the subpopulation of subthreshold neurons is higher than the degree of sparse spike synchronization $M_c^{(\mathrm{supra})}$ in the subpopulation of suprathreshold neurons. This can be understood from the oscillating patterns of the global and the individual potentials. The global potentials V_{supra} and V_{sub} exhibit small regular oscillations (see figures 3(*a*2)–(*a*5) and figures 3(*c*3)–(*c*5)). Like the case of the global potential, the individual subthreshold neurons exhibit only coherent subthreshold hoppings, in contrast to the case of suprathreshold neurons exhibiting both the coherent sparse spikings and the coherent hoppings. Hence, the cross-correlations between V_{sub} and the individual potentials of subthreshold neurons become higher than those between V_{supra} and the individual potentials of suprathreshold neurons. Thus,

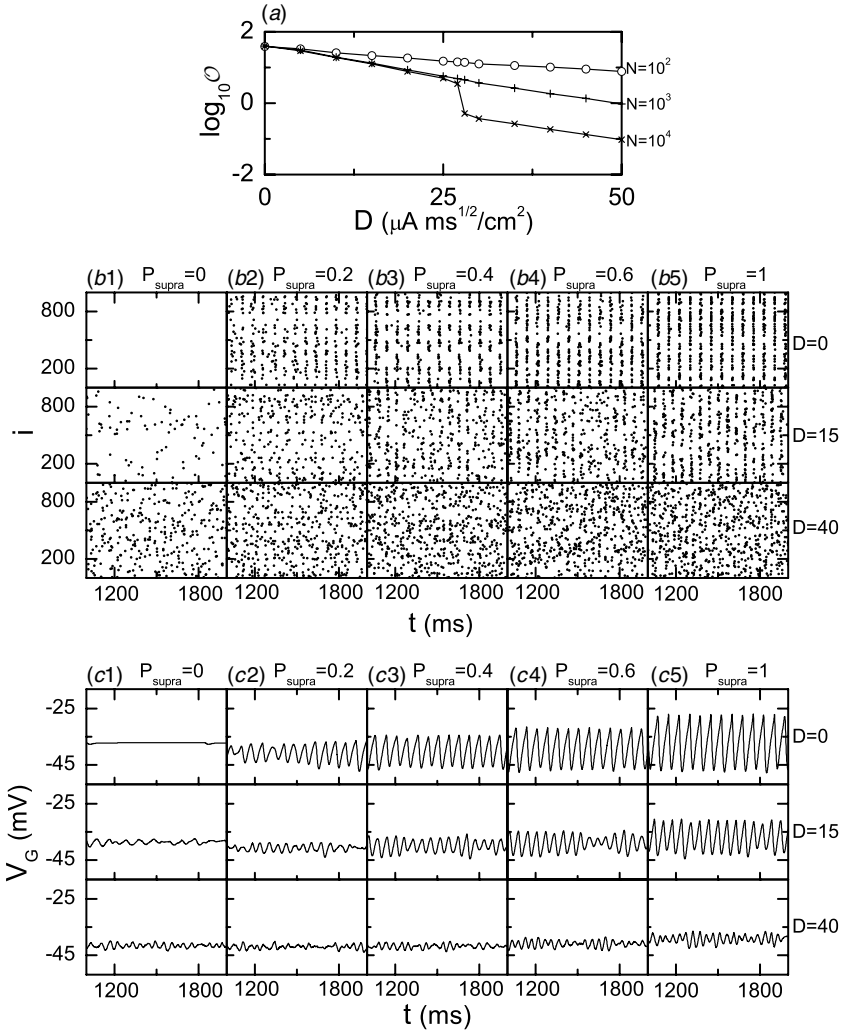

Figure 5. (*a*) Plots of the order parameter $\mathcal{O}$ versus the noise intensity D for $P_{\rm supra} = 1$, (*b*1)–(*b*5) raster plots of neural spikes and (*c*1)–(*c*5) global potentials V_G for various values of $P_{\rm supra}$ and D in a heterogeneous ensemble of N globally coupled subthreshold and suprathreshold type-I ML neurons for $J = 20$ mS cm^{-2}; $N = 10^3$ in (*b*1)–(*b*5) and (*c*1)–(*c*5). The value of $I_{{\rm dc},i}$ for each subthreshold (suprathreshold) type-I ML neuron is randomly chosen with a uniform probability in the range of $(I^*_{\rm dc} - \Delta, I^*_{\rm dc})$ $((I^*_{\rm dc}, I^*_{\rm dc} + \Delta))$, where $I^*_{\rm dc} = 40$ μA cm^{-2} and $\Delta = 10$ μA cm^{-2}.

the correlation-based coherence measure represents the degree of hopping synchronization of subthreshold neurons very well.

In the above, we study the inhibitory coherence for a fixed value of $D = 8$, where $P^*_{\rm supra} \simeq 0.16$. By varying the noise intensity D, we briefly investigate the effect of noise on the inhibitory coherence for $J = 20$. For $P_{\rm supra} = 1$, plots of the order parameter $\mathcal{O}$ versus D are shown in figure 5(*a*). The degree of inhibitory coherence decreases monotonically with increasing D from zero, and a transition to an incoherent state occurs when passing a threshold D^* ($\simeq 28$). Figures 5(*b*1)–(*b*5) and (*c*1)–(*c*5) show the raster plots of spikes and the global potentials V_G for various values of D and $P_{\rm supra}$. For $P_{\rm supra} = 1$, with increasing D, the stripes

in the raster plot become more smeared and the amplitude of V_G decreases. Eventually, when passing the threshold D^*, incoherent states appear (i.e. the raster plot consists of randomly scattered spikes and V_G exhibits a nearly stationary irregular oscillation). Hence, as D is increased, the value of $P^*_{\rm supra}$ (the threshold value of the fraction of suprathreshold neurons for the emergence of inhibitory coherence) increases; $P^*_{\rm supra} = 0.08$ and 0.28 for $D = 0$ and 15, respectively. Thus, for $D > D^*$, no inhibitory coherence emerges, as shown in the case of $D = 40$.

So far, we consider the globally coupled case. However, in a real brain, each neuron is coupled to only a certain number of neurons, which is much smaller than the total number of neurons. Due to the sparseness of the network architecture, the inhibitory coherence (seen in the globally coupled case) is expected to be reduced or destroyed. It is often assumed in models that the coupling between neurons is random [11, 16, 42–44]. We briefly investigate the effect of sparse random connectivity on the inhibitory coherence for $J = 20$ and $D = 8$ by varying the average number of synaptic inputs per neuron $M_{\rm syn}$ in a heterogeneous ensemble of N randomly coupled subthreshold and suprathreshold type-I ML neurons. Figures 6(a1)–(a5) and (b1)–(b5) show the raster plots of spikes and the global potentials V_G for various values of $M_{\rm syn}$ and $P_{\rm supra}$ when $N = 10^3$. For $P_{\rm supra} = 1$, with decreasing $M_{\rm syn}$, the stripes of spikes in the raster plot become more smeared and the amplitude of V_G decreases. Eventually, incoherent states appear when passing a threshold $M^*_{\rm syn}$ (i.e. the raster plot is composed of randomly scattered spikes and V_G shows a nearly stationary irregular oscillation). Hence, as $M_{\rm syn}$ is decreased from $N - 1$ (corresponding to the globally coupled case), a larger fraction of suprathreshold neurons is necessary for the appearance of inhibitory coherence (e.g., see the cases of $M_{\rm syn}$ =800 and 500). Thus, for $M_{\rm syn} < M^*_{\rm syn}$, inhibitory coherence disappears, as shown in the case of $M_{\rm syn} = 100$. As is well known, $M_{\rm syn}$ (rather than $P_{\rm syn}$ (i.e. the connection probability per neuron)) plays an appropriate sparseness parameter for the coherent transition because there exists a fixed threshold value $M^*_{\rm syn}$ for large N, independent of N [2, 44]. (In contrast, the threshold value of $P_{\rm syn}$ depends on N.) When $P_{\rm supra} = 1$, plots of the order parameter $\mathcal{O}$ versus the effective average number of synaptic inputs per neuron $M_{\rm syn,eff}$ ($1/M_{\rm syn,eff} = 1/M_{\rm syn} - 1/N$) are shown in figure 6($c$) for $N = 100, 300, 500, 1000$ and 3000, where the correction term ($\sim 1/N$) takes into account the finite network size effect [2, 44]. Inhibitory coherence emerges when $M_{\rm syn,eff}$ is larger than a threshold $M^*_{\rm syn,eff}$ ($\simeq 553$); for the case of $N = 10^3$, $M^*_{\rm syn} \simeq 356$.

4. Summary

We are concerned about inhibitory coherence in a population of type-I neurons. Both the subthreshold and the suprathreshold neurons coexist in a noisy environment of a real brain. Hence, we consider a heterogeneous population of globally coupled subthreshold and suprathreshold type-I ML neurons and investigate inhibitory coherence by increasing the fraction of suprathreshold neurons $P_{\rm supra}$. For $P_{\rm supra} = 0$, no inhibitory coherence has been observed, which implies that subthreshold type-I neurons are difficult to synchronize by synaptic inhibition. However, as $P_{\rm supra}$ passes a threshold value $P^*_{\rm supra}$, a coherent transition occurs in the subpopulation of suprathreshold neurons, and these synchronized suprathreshold neurons play the role of coherent inhibitors for the emergence of inhibitory coherence in the whole heterogeneous population. Consequently, for $P_{\rm supra} > P^*_{\rm supra}$, a regular population rhythm with a small amplitude appears in the population-averaged global potential. For this coherent case, suprathreshold neurons exhibit sparse spike synchronization (i.e. both the coherent sparse spiking and the coherent subthreshold small-amplitude hopping phases

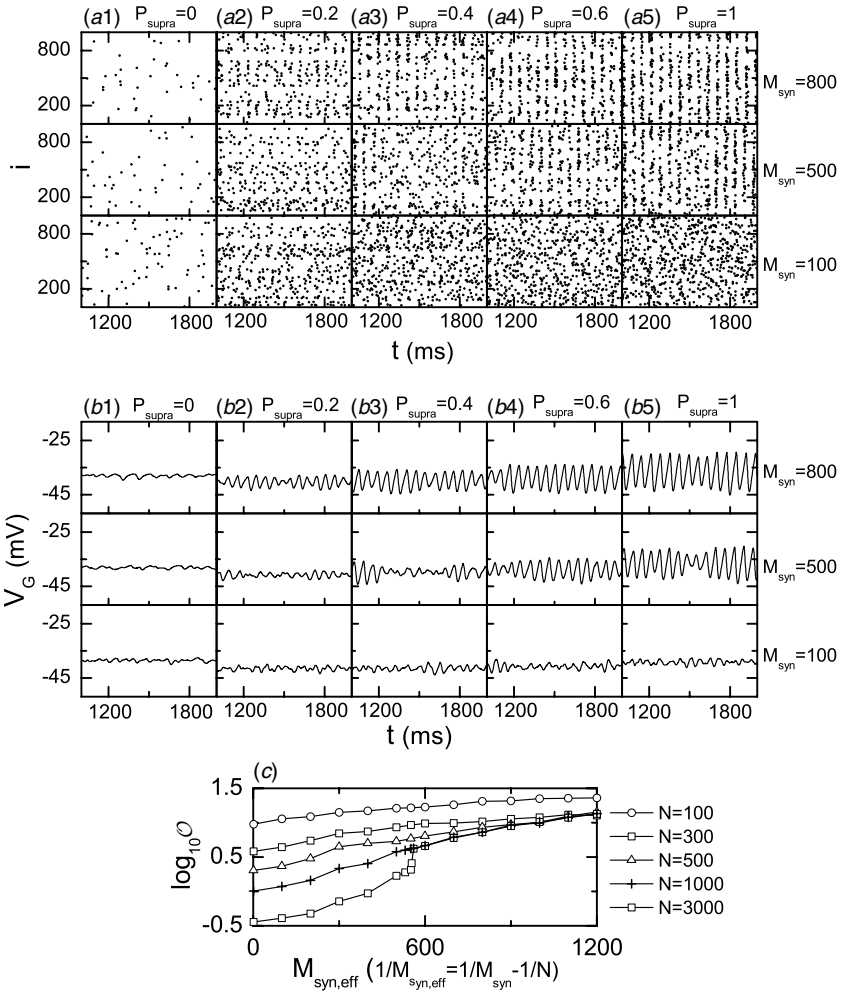

Figure 6. (*a*1)–(*a*5) Raster plots of neural spikes and (*b*1)–(*b*5) global potentials V_G for various values of P_{supra} and M_{syn} in a heterogeneous ensemble of N ($= 10^3$) randomly coupled subthreshold and suprathreshold type-I ML neurons for $J = 20$ mS cm^{-2} and $D = 8$ μA ms$^{1/2}$ cm^{-2}. (*c*) Plots of the order parameter $\mathcal{O}$ versus the effective average number of synaptic inputs per neuron $M_{\text{syn,eff}}$ ($1/M_{\text{syn,eff}} = 1/M_{\text{syn}} - 1/N$) for $P_{\text{supra}} = 1$. The value of $I_{\text{dc},i}$ for each subthreshold (suprathreshold) type-I ML neuron is randomly chosen with a uniform probability in the range of $(I^*_{\text{dc}} - \Delta, I^*_{\text{dc}})$ $((I^*_{\text{dc}}, I^*_{\text{dc}} + \Delta))$, where $I^*_{\text{dc}} = 40$ μA cm^{-2} and $\Delta = 10$ μA cm^{-2}.

appear in the individual potentials of suprathreshold neurons). By virtue of their coherent inhibition, sparsely synchronized suprathreshold neurons suppress the noisy activity of subthreshold neurons. Hence, subthreshold neurons exhibit hopping synchronization (i.e. only the coherent fast subthreshold hopping phase appears in the individual potentials of subthreshold neurons.) We have also characterized the inhibitory coherence in terms of the 'statistical-mechanical' coherence measures based on spikes and correlations, which quantify the average contributions of the microscopic individual spikes and individual potentials to the macroscopic global potential. Thus, sparse spike synchronization of suprathreshold neurons and hopping synchronization of subthreshold neurons have been well characterized in terms of

the spike-based and the correlation-based coherence measures, respectively. Finally, the effect of sparse random synaptic connectivity on the inhibitory coherence has been investigated, and the emergence of inhibitory coherence has thus been found to persist only if the average number of synaptic inputs per neuron $M_{\rm syn}$ is larger than a threshold value $M^*_{\rm syn}$. This kind of inhibitory coherence that emerges from sparsely synchronized oscillations of suprathreshold neurons might be associated with cortical rhythms with irregular and sparse neural firings, which contribute to cognitive functions such as information integration, working memory and selective attention [2, 37].

Acknowledgments

This research was supported by the Basic Science Research Program through the National Research Foundation of Korea funded by the Ministry of Education, Science and Technology (2010-0015730).

References

[1] Buzsáki G 2006 *Rhythms of the Brain* (New York: Oxford University Press)
[2] Wang X-J 2010 *Physiol. Rev.* **90** 1195
[3] Gray C M 1994 *J. Comput. Neurosci.* **1** 11
[4] Hauschildt B, Janson N B, Balanov A and Schöll E 2006 *Phys. Rev.* E **74** 051906
Grosse P, Cassidy M J and Brown P 2002 *Clin. Neurophysiol.* **113** 1523
Tass P, Rosenblum M G, Weule J, Kurths J, Pikovsky A, Volkmann J, Schnitzler A and Freud H J 1998 *Phys. Rev. Lett.* **81** 3291
[5] Wang X-J 2003 *Encyclopedia of Cognitive Science* ed L Nadel (London: Macmillan) pp 272–80
[6] Bremer F 1958 *Physiol. Rev.* **38** 357
Traub R D, Miles R and Wong R K S 1989 *Science* **243** 1319
[7] van Vreewijk C, Abbott L F and Ermentrout G B 1994 *J. Comput. Neurosci.* **1** 313
[8] Hansel D, Mato G and Meunier C 1995 *Neural Comput.* **7** 307
[9] Wang X-J and Rinzel J 1992 *Neural Comput.* **4** 84
[10] Golomb D and Rinzel J 1994 *Physica* D **72** 259
[11] Wang X-J and Buzsáki G 1996 *J. Neurosci.* **16** 6402
[12] White J, Chow C C, Ritt J, Soto-Trevino C and Kopell N 1998 *J. Comput. Neurosci.* **5** 5
[13] Whittington M A, Traub R D, Kopell N, Ermentrout B and Buhl E H 2000 *Int. J. Psychophysiol.* **38** 315
[14] Tiesinga P H E, Fellous J-M, Jose J V and Sejnowski T J 2001 *Hippocampus* **11** 251
[15] Hansel D and Mato G 2003 *Neural Comput.* **15** 1
[16] Börgers C and Kopell N 2003 *Neural Comput.* **15** 509
Börgers C and Kopell N 2005 *Neural Comput.* **17** 557
[17] Buzsáki G, Geisler C, Henze D A and Wang X-J 2004 *Trends Neurosci.* **27** 186
Yu S, Huang D, Singer W and Nikolie D 2008 *Cereb. Cortex* **18** 2891
Wang Q, Duan Z, Perc M and Chen G 2008 *Europhys. Lett.* **83** 50008
Roxin A, Riecke H and Solla S 2004 *Phys. Rev. Lett.* **92** 198101
Riecke H, Roxin A, Madrugs S and Solla S 2007 *Chaos* **17** 026110
Wang Q, Perc M, Duan Z and Chen G 2010 *Physica* A **389** 3290
[18] Wang Q, Perc M, Duan Z and Chen G 2009 *Phys. Rev.* E **80** 026206
Morgan R and Soltesz I 2008 *Proc. Natl Acad. Sci. USA* **105** 6179
Wang Q, Chen G and Perc M 2011 *PLoS One* **6** e15851
[19] Sun X, Lei J, Perc M, Kurths J and Chen G 2011 *Chaos* **21** 016110
[20] Hodgkin A L 1948 *J. Physiol.* **107** 165
[21] Rinzel J and Ermentrout B 1998 *Methods in Neural Modeling: From Ions to Networks* ed C Koch and I Segev (Cambridge, MA: MIT Press) p 251
[22] Izhikevich E M 2000 *Int. J. Bifurcation Chaos* **10** 1171
[23] Hansel D, Mato G and Meunier C 1995 *Neural Comput.* **7** 307
[24] Marella S and Ermentrout G B 2008 *Phys. Rev.* E **77** 041918
Ermentrout B 1996 *Neural Comput.* **8** 979

[25] Izhikevich E M 1999 *IEEE Trans. Neural Netw.* **10** 499
[26] Mato G and Samengo I 2008 *Neural Comput.* **20** 2418
[27] Malik N, Ashok B and Balakrishnan J 2010 *Pramana J. Phys.* **74** 189
[28] Connor J A and Stevens C F 1971 *J. Physiol.* **213** 31
[29] Hindmarsh J L and Rose R M 1984 *Proc. R. Soc.* B **221** 87
[30] Morris C and Lecar H 1981 *Biophys. J.* **35** 193
[31] Spencer K M, Nester P G, Niznikiewicz M A, Salisbury D F, Shenton M E and McCarley R W 2003 *J. Neurosci.* **23** 7407
[32] Uhlhaas P J and Singer W 2010 *Nature Rev. Neurosci.* **11** 100
[33] Volman V, Behrens M M and Sejnowski T 2011 *J. Neurosci.* **31** 18137
[34] Wang Y, Chik D T W and Wang Z D 2000 *Phys. Rev.* E **61** 740
[35] Lim W and Kim S-Y 2007 *J. Korean Phys. Soc.* **51** 1427
Lim W and Kim S-Y 2009 *Int. J. Mod. Phys.* B **23** 703
[36] Lim W and Kim S-Y 2011 *J. Comput. Neurosci.* **31** 667
Hong D-G, Kim S-Y and Lim W 2011 *J. Korean Phys. Soc.* **59** 2840
[37] Brunel N and Hakim V 2008 *Chaos* **18** 015113
Brunel N and Hakim V 1999 *Neural Comput.* **11** 1621
Brunel N 2000 *J. Comput. Neurosci.* **8** 183
Brunel N and Wang X-J 2003 *J. Neurophysiol.* **90** 415
Geisler C, Brunel N and Wang X-J 2005 *J. Neurophysiol.* **94** 4344
[38] Lim W and Kim S-Y 2010 *J. Korean Phys. Soc.* **57** 1290
[39] San Miguel M and Toral R 2000 *Instabilities and Nonequilibrium Structures VI* ed J Martinez, R Tiemann and E Tirapegui (Dordrecht: Kluwer) p 35
[40] Manrubia S C, Mikhailov A S and Zanette D H 2004 *Emergence of Dynamical Order* (Singapore: World Scientific)
[41] Freund J, Schimansky-Geiser L and Hänggi P 2003 *Chaos* **13** 225
[42] Barkai E, Kanter I and Sompolinky H 1990 *Phys. Rev.* A **41** 590
[43] Wang X-J, Golomb D and Rinzel J 1995 *Proc. Natl Acad. Sci.* **92** 5577
[44] Golomb D and Hansel D 2000 *Neural Comput.* **12** 1095